Research article

Seemesh Bhaskar, Pratyusha Das, Maku Moronshing, Aayush Rai, Chandramouli Subramaniam*, Shivakiran B. N. Bhaktha* and Sai Sathish Ramamurthy*

Photoplasmonic assembly of dielectric-metal, Nd_2O_3-Gold soret nanointerfaces for dequenching the luminophore emission

https://doi.org/10.1515/nanoph-2021-0124
Received March 23, 2021; accepted August 6, 2021; published online August 20, 2021

Abstract: A variety of materials such as low dimensional carbon substrates (1D, 2D, and 3D), nanoprisms, nanocubes, proteins, ceramics, and DNA to name a few, have been explored in surface plasmon-coupled emission (SPCE) platform. While these offer new physicochemical insights, investigations have been limited to silver as primary plasmonic material. Although, gold nanoparticles (AuNPs) exhibit robust performance, its intrinsic property to quench the emission from radiating dipoles (at distances < 5 nm) has impeded its utility. Despite the use of metal-dielectric resonances (with Au decorated SiO_2 NPs) and sharp nanotips (from Au nanostars) for dequenching the emission, the enhancements obtained has been less than 200-fold in SPCE platform. To address these long-standing challenges, we demonstrate the utility of gold soret colloids (AuSCs) and photonic crystal-coupled emission (PCCE) platform. The soret nano-assemblies synthesized using adiabatic cooling technique presented integrated hotspots when taken with high refractive index Nd_2O_3 'Huygens sources'. The collective and coherent coupling between localized Mie and delocalized Bragg plasmons (of sorets), dielectric plasmons (of Nd_2O_3), highly confined and intense Bloch surface waves (of PCCE platform) aided in realization of dequenched, as well as amplified > 1500-fold enhancements at the photoplasmonic nanocavity interface, presenting new opportunities for multidisciplinary applications.

Keywords: cavity nanointerface; dequenching; fluorescence; photonic crystal; plasmonics; soret colloid.

1 Introduction

Nanophotonics, nanoplasmonics and their synergistic combination play a central role in the emerging technological revolution [1–7]. Although various types of nanoparticles (NPs) have been explored for different applications, gold (Au) NPs have gained significant attention on account of their unique optical, electronic and chemical properties [8]. The large electron densities of $\approx 5.9 \times 10^{22}\ cm^{-3}$ (with ≈6 Å average distance travelled per oscillation time period) in gold result in copious oscillating electrons (plasmons) and extremely high electric field enhancement at their surface in near-field [8–11]. The concept of 'hotspot', that can be generated between adjacent NPs or NP and thin film with regard to gold has resulted in numerous applications.

By and large, the scientific field that deals with plasmonics, coupled with spectroscopic techniques, has recently developed into an independent research field known as 'plasmon-enhanced spectroscopy' [3, 4, 12]. Lakowicz and co-workers in the year 2004, established a resourceful tool in this context, termed surface plasmon-coupled emission (SPCE), with >50% highly directional

*Corresponding authors: **Sai Sathish Ramamurthy**, Department of Chemistry, STAR Laboratory, Sri Sathya Sai Institute of Higher Learning, Prasanthi Nilayam, Puttaparthi, 515134, Anantapur, Andhra Pradesh, India, E-mail: rsaisathish@sssihl.edu.in. https://orcid.org/0000-0001-9957-9259; and **Chandramouli Subramaniam**, Department of Chemistry, Indian Institute of Technology Bombay, Powai, Mumbai 400076, Maharashtra, India, E-mail: csubbu@chem.iitb.ac.in. http://orcid.org/0000-0001-8335-7395; and **Shivakiran B. N. Bhaktha**, Department of Physics, Indian Institute of Technology Kharagpur, Kharagpur 721302, India, E-mail: kiranbhaktha@phy.iitkgp.ac.in. http://orcid.org/0000-0003-4846-8262
Seemesh Bhaskar and Aayush Rai, Department of Chemistry, STAR Laboratory, Sri Sathya Sai Institute of Higher Learning, Prasanthi Nilayam, Puttaparthi, 515134, Anantapur, Andhra Pradesh, India. https://orcid.org/0000-0003-2714-3776 (S. Bhaskar). https://orcid.org/0000-0001-8853-7715 (A. Rai)
Pratyusha Das, Department of Physics, Indian Institute of Technology Kharagpur, Kharagpur 721302, India. http://orcid.org/0000-0003-3067-421X
Maku Moronshing, Department of Chemistry, Indian Institute of Technology Bombay, Powai, Mumbai 400076, Maharashtra, India. http://orcid.org/0000-0001-9169-0745

and polarized emission signal collection efficiency (vis-à-vis <1% in conventional luminescence) [3, 6, 13]. The SPCE platform has been used to study different applications ranging from real-time polymerization process [14], waveguide properties [15], excitation–emission synchronization [16], monomer-higher order aggregates energy transfer [17], cardiac marker myoglobin immunoassay [18], kinetics of adsorption [19] and polymer light-emitting diodes [20], to name a few.

Furthermore, new experimental and theoretical parameters have been discussed in SPCE, along with insightful biophysicochemical concepts [21–24]. In spite of their versatile functionalities, SPR, SPCE, metal-dielectric-metal (MDM) [25] and Tamm state-coupled emission (TSCE) technologies [26], suffer from inevitable dissipative Ohmic losses due to metal-dependent subject platform [5]. While this is the primary concern for biosensing applications, the study and utility of AuNPs (unlike other coinage metals) in SPCE has been a long-standing challenge on account of its quenching phenomenon [27, 28]. In our recent investigations, dielectric SiO_2 NPs decorated with AuNPs (AuSil) [29] and highly sharp-edged Au nanostars (AuNS) [30] have been examined to dequench the otherwise quenched molecular fluorescence. That is, we have accomplished SPCE substrate engineering to utilize the functionality of metal-dielectric resonances (in AuSil) and intense hotspots (in AuNS) in order to circumvent the quenching phenomenon. Nevertheless, the emission enhancements achieved have been <200-fold [29, 30], on account of the incompetence of SPCE to further augment the dequenched emission. Therefore, one can notice that although we could realize dequenched emission with the use of substrate engineering, there is a trade-off using the SPCE platform [29, 30].

In order to address these dual limitations of loss in SPCE platform and quenching with the usage of AuNPs, in this report, we propose the utility of photonic crystal-coupled emission (PCCE) platform [31, 32]. PCCE platform presents one-dimensional photonic crystal (1DPhC) as an essential lossless analogue to SPCE platform with exceptional advantages over it [32]. Single-molecule detection (at zeptomolar concentration) of stress hormone, cortisol has been achieved experimentally thereby confirming PCCE as a particularly powerful technique [32]. In light of this background, here we observed that the use of AuNPs in PCCE platform presented dequenched and enhanced emission (278-fold enhancements), that has not been reported hitherto.

Furthermore, efforts to obtain dequenched emission using AuSil and AuNS demands experimental expertise and skill in synthesis, thereby making them complex and non-user-friendly [29, 30]. In the case of AuSil, the clustering/assembling effect of AuNPs was the ingenuity achieved on SPCE substrate engineering (for generating abundant hotspots) along with metal-dielectric resonances towards overcoming the quenching phenomenon [29]. In this work, we intended to explore the utility of soret colloids (SCs) of pristine nanomaterials [33]. Thermomigrative assembly of homogeneous metal NPs under adiabatic conditions have been established to yield highly monodisperse NP assembly, termed as SCs [33, 34]. The time period of such adiabatic cooling provides a unique and convenient methodology to precisely control the number of NPs per SC, enabling SC60, SC90 and SC120 with compositions of 9 (±3), 19 (±3) and 48 (±4) number of NPs [33–35]. Moreover, the detailed mechanism and validation of the protocol is presented in our earlier works where monodispersity of these NPs assemblies have been discussed, establishing the precise control that can be obtained with different cooling times [33–35]. Such thermomigratively assembled SCs represent non-chemical, linker-free assembly of NPs and thus represent a unique advantage over other conventional methods that rely on chemical functionalization for NPs assembly. The resulting SCs have yielded uniform and high density of electromagnetic hotspots leading to ultra-sensitive, single-molecular level detection capabilities as both SERS and SPCE platforms [33–35]. Additionally, silver sorets have been extensively studied in SPCE platform toward Purcell-enhanced femtomolar sensing of a biologically relevant molecule (glutathione) with excellent reliability [21].

In light of these observations, the adiabatic cooling technique was employed to fabricate stable, predefined assemblies of AuNPs, termed gold soret colloids (AuSCs) to comprehend their efficacy toward dequenching. The compositional effect of SC on the dequenching ability in SPCE platform is investigated in detail, by employing SC60, SC90 and SC120 of AuNPs [33–36]. In light of substrate engineering accomplished using the SPCE platform, we have designed different nanointerfaces (spacer, cavity and extended [ext.] cavity nanointerfaces) as reported earlier [21–24, 29–32]. Experimental evidence for better coupling efficiency from SC90 (>160-fold) as compared to SC60 (>70-fold) and SC120 (>90-fold) in cavity interface has been demonstrated. For the first time, to the best of our knowledge, engineering of cavity nanointerface with SC90 on PCCE platform presented dequenched >800-fold emission enhancement (vis-à-vis dequenched 278-fold from pristine AuNPs). While we deliberated on comparing and contrasting the performance of SPCE and PCCE platforms using AuNPs and AuSC, the obtained emission enhancements are still not excessive as compared to existing literature [32]. In our

recent report [32], we noted that high refractive index (HRI) dielectric (Nd_2O_3) nanorods (NRs), when taken in combination with nanoprisms presented augmented >1300-fold PCCE enhancement. HRI dielectric NRs act as efficient 'Huygen sources' displaying augmented forward scattering and amplified coupling with propagating plasmons of metal thin film [22, 36–39]. Hence, in this report, we present the synergistic combination of metal-AuSC and dielectric-HRI Nd_2O_3 NRs to realize >1500-fold emission enhancements using the PCCE platform (vis-à-vis >360-fold in SPCE). The utilization of metal nano-assembly (with intense localized and delocalized plasmons) [40], HRI dielectric NRs, Bloch surface waves (BSWs) from PCCE platform with intense and integrated hotspots was designed to achieve this ultra-amplification in emission enhancements. The highly directional and polarized emission obtained experimentally is supported using TFCalc simulations. The dequenched and augmented emission using AuSC presented in this work is anticipated to be of immediate use for interdisciplinary applications, including biosciences (genomics, proteomics, and diagnostics), chemical sensing, materials science and photonics.

2 Experimental section

The experimental framework used in our work involves reverse Kretschmann (RK) configuration where the laser light illuminates the engineered SPCE or PCCE substrates directly from the free space (FS) side (and not from the prism side) (Supplementary material). The SPCE and PCCE substrates include 50 nm Ag thin film and 1DPhC, respectively. The coupling of the radiating dipoles with the SPCE and PCCE substrates are presented in Figure 1a and b, respectively. One can also observe the magnified conceptual schematics presenting the coupling phenomenon between the emitter dipoles and surface plasmons of SPCE substrate (Figure 1a) and also between emitter dipoles, BSWs and internal optical modes (IOMs) of PCCE substrate (Figure 1b). The angle of incidence (in Kretschmann configuration) at which the evanescent field is generated in the metal-dielectric interface in conventional surface plasmon resonance (SPR) technique is considered as the angle at which the fluorescence emission can be expected in SPCE technology [3, 4]. In other words, this is the angle of minimum reflectivity of the interface. In SPCE experimentation, for coupling of surface plasmons to occur with emitter dipoles, the surface plasmon polariton (SPP) dispersion relation [3, 4, 13], given by equation (1), needs to be satisfied:

$$k_{\mathrm{SPP}} = \frac{\omega}{c}\sqrt{\frac{\epsilon_m \epsilon_d}{\epsilon_m + \epsilon_d}} \tag{1}$$

This equation is affected by the variation of the dielectric properties placed over the metal thin film. Here, ε_m and ε_d are the dielectric functions/relative permittivities of the metal and dielectric layers respectively (Figure 1a), ω and c are the angular frequency and speed of light in vacuum. Also, k_{SPP} is the wave vector of SPP propagating along the interface between the metal and the dielectric. As

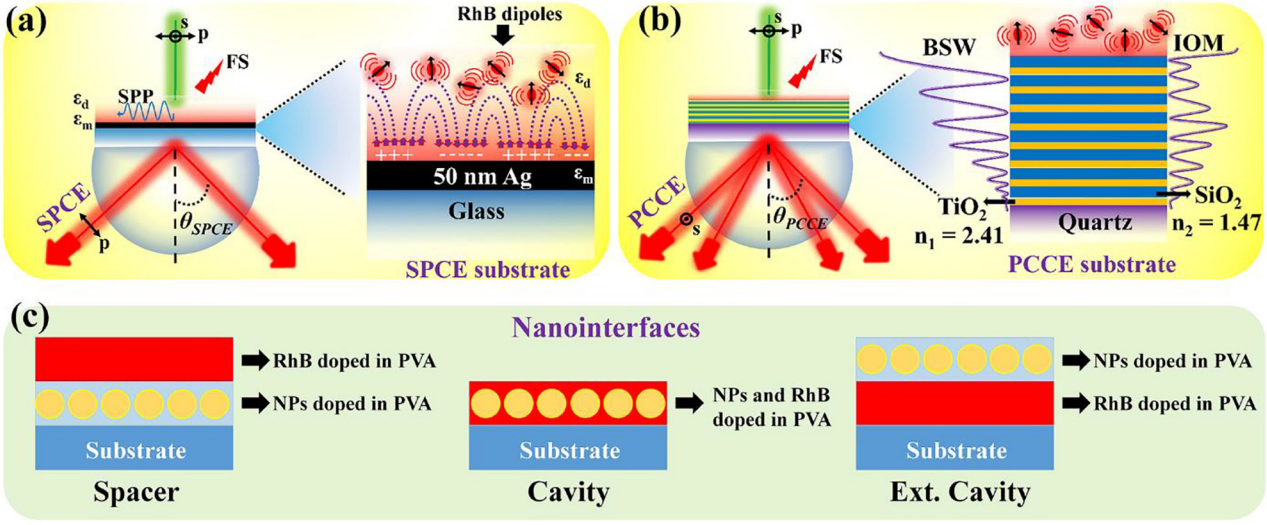

Figure 1: Conceptual schematic of coupling of emission with (a) propagating surface plasmon polaritons (SPPs) of metal thin film (with θ_{SPCE} as the angle of emission) and (b) surface-trapped modes of 1DPhC (with θ_{PCCE} as angle of emission). The magnified images on the right side of (a) and (b) display the coupling at the nanointerface. (c) Schematic representation of spacer, cavity and ext. cavity nanointerfaces. Additional details are presented in Supplementary material.

a result of this relationship, the angle of minimum reflectivity or maximum coupling of fluorescence with surface plasmons (θ_{SPCE}) can be modified by changing the dielectric constants of materials under study. That is substrate engineering by doping the dielectric nanolayer with NPs of interest results in modulation of the angle of emission maxima, as elaborated in subsequent sections.

Furthermore, in order to maintain generality across experiments, we have used poly-vinyl alcohol (PVA) as the dielectric material for doping the radiating dipoles. The nanomaterials considered and their sorets possess different surface potentials and sizes, as detailed in the zeta potential measurements and TEM images in subsequent sections. Additionally, equal quantities of AuNPs, SC60, SC90 and SC120 have been doped in the PVA matrix for SPCE and PCCE experimentation in order to draw comparative and logical conclusions across the experimental results. This is in accordance with the experimental study performed with silver soret colloids in our recent work [21]. An index matching fluid glycerol (RI = 1.47) was used for fixing the nanoengineered SPCE substrates to a hemicylindrical prism. Nanoengineering is undertaken by the fabrication of spacer, cavity and ext. cavity nanointerfaces with and without NPs of interest. The conceptual schematic of these nanointerfaces are presented in Figure 1c, and the details are elaborated in our earlier reports [21–24, 29–32]. In brief, the spacer nanointerface consists of NPs doped PVA (30 nm) used as a spacer layer between the substrate and radiating dipoles doped PVA (30 nm). In the cavity, the radiating dipoles are sandwiched in the infinitesimal nanogaps between the substrate and the NPs. This cavity nanointerface is obtained by admixing the NPs and radiating dipoles and spin coating as a single layer on the substrate. In ext. cavity configuration [22], a gap between the NPs and the substrate is introduced (30 nm in this work) to understand the long-distance coupling attributes. Also, we note that the MDM nanointerface is exceedingly desirable for steering of emission into direction normal to the surface, that is of utility for biomedical applications [25]. Although we have not observed a similar emission pattern (normal to the substrate), SCs on account of nano-assembly architecture, while taken on SPCE platform in ext. cavity interface partially resembles MDM nanointerface [21]. Hence, it can also be called pseudo-MDM.

Also, the fabrication details of 1DPhC along with cross-sectional imaging and experimental reflectance data is presented in our recent report [31]. An illumination light source of 532 nm, 30 mW continuous wave (CW) laser excitation was incident onto the fabricated substrates, and the coupled emission was collected from distal part of the prism. A 550 nm long wave pass (LWP) filter was used for the collection of emission from the plasmonic substrates upon direct excitation with the laser source. Both the free space (FS) and coupled emission (from SPCE and PCCE platforms) were recorded using USB4000 fiber optic spectrometer connected to Ocean Optics SpectraSuite software. A sheet polarizer was placed in between the prism and fiber optic collector in vertical and horizontal orientations to capture polarized emissions (p and s polarized emission). The emission enhancements calculated as the ratio of SPCE or PCCE intensity to FS intensity, directionality of angular emission and polarization aspects were determined for all the samples. 1 mM RhB dispersed in PVA matrix (2 wt%) was spin coated at 3000 rpm for 1 min to obtain ~60 nm PVA thin films [22, 31, 32].

Throughout our experiments, we have used AuNPs synthesized using the conventional Turkevitch method [41, 42]. Details of AuSCs synthesized using the adiabatic cooling technique is presented in detail in earlier works [34, 35]. The conceptual schematic explaining the synthesis methodology is presented in Figure 2a. In brief, the adiabatic cooling time of AuNPs was tailored from 60 to 90 to 120 min to obtain nano-assemblies with increasing number of AuNPs, which we have termed SC60, SC90 and SC120 respectively. Morphological and structural characterization of the synthesized AuSCs was performed using transmission electron microscopy (TEM; 300 kV, Tecnai G2, F30). Dynamic light scattering (DLS) experiments and zeta potential measurements were performed using Anton Paar Particle analyzer (Litesizer™ 500, DLS-based particle analyzer).

3 Results and discussion

The detailed analysis of spectrophotometric absorbance of AuNPs, along with gold SC60, SC90 and SC120 has been elaborately discussed in our earlier reports [33–35]. In brief, it has been noted that while AuNPs display transverse LSPR, the SCs presented longitudinal absorbance at higher wavelengths on account of inter-plasmon coupling. Further, the size distributions for all SCs were performed using DLS (Figure 2b). The hydrodynamic diameter obtained for AuNPs, SC60, SC90 and SC120 were 21, 280, 466 and 653 nm respectively, indicating an increase in the size of SCs with increasing cooling time. The zeta potential measurements for AuNPs, SC60, SC90 and SC120 were −33, −39, −16 and −8 mV respectively, confirming good stability of the synthesized sorets (Figure 2c). The DLS and zeta potential data obtained herewith are in excellent consonance with earlier reported values [33–35].

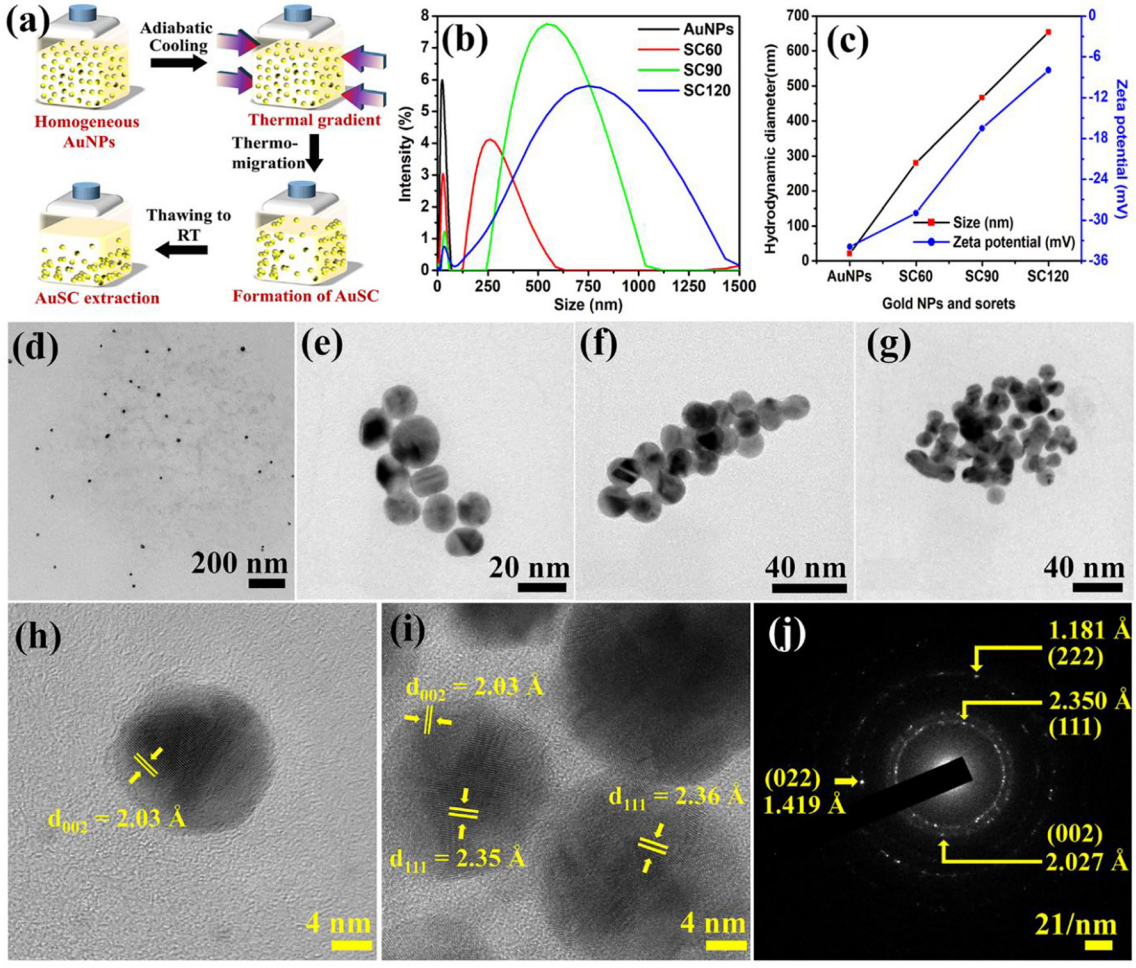

Figure 2: (a) Schematic of adiabatic cooling methodology adopted for synthesis of AuSCs. The steps involved are self-explanatory. (b) DLS size distribution for different AuSCs. (c) Hydrodynamic diameter and zeta potentials for different AuSCs. (d) TEM image of AuNPs used for AuSC synthesis. TEM images of (e) SC60, (f) SC90 and (g) SC120 clearly indicating the increase in the number of AuNPs per soret as we increase the time of adiabatic cooling. (h) HRTEM image of AuNP indicating the lattice fringes characteristic to gold that does not display assembly formation. (i) HRTEM image of AuSC indicating the lattice fringes characteristic to gold that clearly display formation of assemblies with nanovoids and nanocrevices. (j) SAED pattern of AuSC presenting bright spots characteristic to that of gold.

The TEM image of AuNPs used for the synthesis of NP assemblies are shown in Figure 2d. Further, the nano-assemblies SC60, SC90 and SC120 of AuNPs are shown in Figure 2e, f, and g. In line with earlier reports [33–35], the SC60, SC90 and SC120 contain 9 (±3), 19 (±3) and 48 (±4) number of AuNPs per soret. Importantly, we note that the number of nanovoids and nanocrevices in and around the NP assembly in sorets increases from SC60 to SC90 to SC120. Furthermore, it is pertinent to observe the morphology of these SCs, where we note that SC60 presents predominantly planar configuration (two-dimensional) due to non-stacking property. On the other hand, SC90 and SC120 presents three-dimensional stacking behavior, as detailed in our recent work on sorets of silver [21]. While the HRTEM image of AuNP presented in Figure 2h displays non-aggregating behavior, the HRTEM images of AuSC presents (in Figure 2i) nano-assembly with nanoscopic gaps between the AuNPs for individual soret. The lattice fringes clearly indicate characteristic d-spacing corresponding to face centered cubic (FCC) gold (ICSD reference code: 98-061-1625, according to which the d-spacing of 2.35097, 2.03600, 1.43967, 1.22775 and 1.17549 corresponds to the Miller indices (111), (002), (022), (113) and (222) respectively). The selected area electron diffraction (SAED) pattern presented in Figure 2j shows bright circular spots that are characteristic of highly crystalline FCC gold NPs (the *d*-spacing along with respective Miller indices are shown in the figure).

All the sorets synthesized above were interfaced with continuous propagating surface plasmons of Ag thin film

in SPCE platform to understand their plasmonic coupling attributes. The experimentally obtained emission enhancements with the use of SC60, 90 and 120 in all the three nanointerfaces are presented in Figure 3a. The blank measurements obtained for samples without any NPs or sorets presented 13, 10 and 8-fold emission enhancements in spacer, cavity and ext. cavity nanointerface respectively, in line with earlier findings [21–24, 29–32]. Incorporating pristine AuNPs resulted in 8, 5 and 15-fold enhancements for spacer, cavity and ext. cavity nanointerfaces. As reported [29, 30] we conclude that AuNPs significantly quenched the emission as compared to blank measurements. Interestingly, largely dequenched emission enhancements were observed with the use of sorets. In spacer nanointerface, the enhancements decreased from 130 to 80 to 32 for SC60, 90 and 120 samples respectively. As reported [21], plasmonic coupling of silver sorets (AgSC60, 90 and 120) in SPCE platform have presented similar trend in results. In brief, such a decrease in enhancements were observed on account of increasing size effects from SC60 to SC90 and SC120, which would lead to projection of bigger sized sorets into FS medium (resulting in lessened plasmonic coupling). Further, results from cavity and ext. cavity nanointerfaces indicate that SC90 presented optimum number of inter, intra nanovoids and crevices [21] for maximum coupling of radiating dipoles with the SPPs of Ag thin film. From the TEM images we note that while SC60 presents predominantly two-dimensional morphology, SC90 and SC120 display three-dimensional stacking of NPs. This in turn would present substantially large number of nanogaps, nanovoids and nanocrevices (please note: nanogap is the gap between the soret and the Ag thin film/substrate; nanovoids are nanogaps within a single cluster/soret; nanocrevices are the nanospaces generated at the external surface morphology of each soret on account of clustering behavior. Further details of these aspects are elaborately presented in earlier work with silver sorets) [21]. However, the size of SC120 is much larger than the 60 nm film of PVA, in which they are doped resulting in extensive backscattering of light to FS region. In other words, incorporating less stable (zeta potential: −8 mV) SC120 would result in significant difference in dielectric constant and increased FS emission, thereby reducing the enhancements in all the three nanointerfaces.

Consequently, SC90 presented a maximum of 160-fold emission enhancements in cavity nanointerface. This is significantly greater than what could be obtained from silver sorets (90-fold) in cavity nanointerface [21]. Hence, we have not only obtained substantially dequenched emission, but also superior emission with the use of gold SC90. The SPCE, FS, *p* and *s* emission profiles for SC90 sample in cavity nanointerface, which resulted in maximum emission enhancements in presented in Figure 3b. The reflectivity plot obtained theoretically using TFCalc simulations for 60 nm PVA on Ag thin film is shown in Figure 3c.

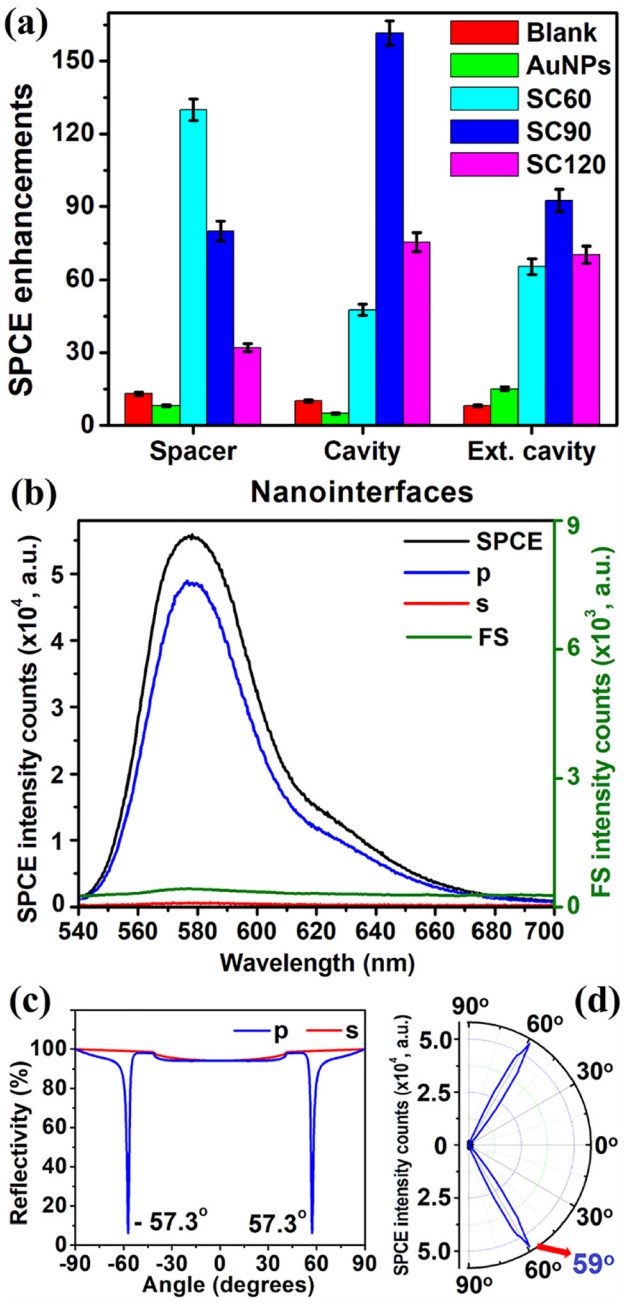

Figure 3: (a) SPCE enhancements, (b) SPCE, Free Space (FS), *p*-polarized (*p*) and *s*-polarized (*s*) emission profiles for the sample that presented maximum emission enhancements in (a) (that is for sample SC90 in cavity nanointerface). (c) Reflectivity plot obtained theoretically. (d) Angularity plot obtained experimentally for sample SC90 in cavity interface.

Furthermore, an excellent agreement is observed for the angularity data obtained experimentally as shown in Figure 3d and the reflectivity plot in Figure 3c. However, as mentioned earlier, doping SC90 in PVA film (dielectric layer) resulted in 2° difference between the theoretical (57.3°) and experimental (59°) data, as it would alter the effective ε_d in equation (1). The highly directional and polarized emission obtained along with dequenched phenomenon from SC90 is of utility in a host of fields including quantum technologies and nano-optics. In this regard, researchers adopt expensive and often cumbersome (with optical components) focusing, reflecting, and/or refracting emission with mirrors and lenses in order to redirect and reshape the far-field emission [43]. While these comprise the geometrical approach, we have adopted cost-effective and reliable near-field beam shaping approach where SPCE platform is utilized to present sharply directional emission to overcome the isotropic fluorescence.

Furthermore, it is important to briefly discuss the incentive for undertaking this research work. For many decades now, it is strongly believed that AuNPs quench the emission from any emitter in the so called "zone of inactivity", while emitters are in their close (<10 nm) vicinity. This is primarily attributed to the coupling of emitters to non-radiative higher-order plasmonic modes which eventually dissipate its energy. However, more recently, it is theoretically and experimentally understood that it is possible to overcome this quenching by placing the emitters in nanocavities where the "quenching is demonstrated to be quenched" due to plasmon mixing or mode hybridization [44–46]. Additionally, hybrid-plasmonic states (superposition of modes) in nanocavities are generated while isolated NPs are brought very close (<5 nm) and also for nearly touching NPs [44]. These higher-order modes acquire a radiative component which massively increases the emitter excitation and decay via radiative channels, thereby presenting enormous increase in emission properties. Additionally, earlier reports [47, 48] suggest that with decreasing the distance between two adjacent AuNPs (or touching NPs) the radiation damping and dephasing of coupled plasmon mode is significantly reduced resulting in colossal increase in the local EM field enhancement in the nanogaps (0–5 nm) between them. Experimental results [48] have confirmed these in the context of fluorescence (560 nm) from emitter placed between AuNP dimers, in direct relevance to our work. Recently, we explored the utility of Au nanostars towards its efficacy in dequenching. However, one must acknowledge the fact that while sharp nanotip morphologies can increase the enhancement factor by 2–3 orders or magnitude, inter-plasmon coupling in inter particle junctions of very closely packed NPs would increase this electric field (EF) intensity by 3–5 orders of magnitude (compared to that observed for isolated NPs) [49]. Moreover, the finite-difference time-domain simulations performed in earlier reports with AgSC confirms the existence of void and cavity plasmons [21]. In a milestone work on fluorescence enhancement with lithographically fabricated bowtie nanoantennas, such FDTD simulations have been comprehensively studied to re-emphasize the importance of nanogaps [50]. In light of these observations, it is pertinent to study the effect of sorets presenting stable NP clusters on metal thin films supporting SPPs. While this was our primary motive, another objective was to explore the effect of three-dimensional hotspots supported by AuSCs. Of late, research is more focused on nanomaterials that sustain three-dimensionally (3D) distributed hotspots, rather than 0D, 1D and 2D distribution of hotspots as the latter is restricted to one or two dimensions sustaining comparatively diminished hotspot density [49]. In light of all these observations, we intended to explore the utility of sorets of gold in SPCE platform which have multiple, nearly touching NPs. More interestingly, sorets present unique nano architectural facets that contain three-dimensionally distributed hotspots catering to uniform and intense EM field enhancements [33–35]. In line with our hypothesis, the obtained emission enhancements (160-fold) for SC90 are significantly higher than silver sorets and many other active plasmonic spacer and cavity materials explored by STAR laboratory in the past (Ag-protein biospacer: 120-fold [31]; PdNPs, Ag-Pd, CNT, graphene: <80-fold [24]; Au-decorated SiO_2 NPs: 88-fold [29]; Au nanostars: 100-fold [30] to name a few. More details are presented in Figure 6).

Although the dequenched emission enhancements obtained with Au sorets in SPCE platform is remarkable, 160-fold is not significantly large to detect very low concentrations of analytes, especially in a biological milieu. For instance, it would demand a strategic methodology to obtain >1000-fold enhancements as in case of earlier works where AgAu nanohybrids [51] and sharp edged Ag nanoprisms with Nd_2O_3 nanorods [32] have been adopted. We note that SPCE platform on account of intrinsic dissipative losses, would compromise on realizing exceptional collection efficiency and in turn, obtaining high emission enhancements. In this regard, we have used PCCE platform to circumvent unavoidable Ohmic losses presented by SPCE platform [31, 32].

The emission enhancements obtained with the use of PCCE platform by considering blank (without any NPs), AuNPs and AuSC90 in cavity nanointerface is presented in Figure 4a. As reported earlier [31, 32], we noted that the enhancements for blank samples were ~35 fold for

BSW-coupled emission. This is ~4 times more than that could be achieved with SPCE platform (5–10 fold) due to negligible losses encountered in PCCE platform. Further, very interesting observations were made by using pristine AuNPs in PCCE vis-à-vis SPCE. Regardless of the well-established quenching of emission by AuNPs, we observed that PCCE platform presented 280-fold emission enhancements for BSW-coupled emission while SPCE platform displayed quenched fivefold enhancements with AuNP in cavity nanointerface. It is relevant to mention that this is more than what has been reported using AgNPs (~200-fold) in the PCCE platform [31].

In addition to this, along with BSW-coupled emission, the first three IOMs sustained by 1DPhC, coupled with the emitter dipoles to show dequenched emission [IOM_1: 132; IOM_2: 123; IOM_3: 32-fold]. The overlap of dispersion diagram obtained numerically (dotted line) and experimentally for AuNPs cavity layer is shown in Figure 4b. Here, the experimental raw data of coupled fluorescence intensity is presented in all the dispersion diagrams in Figure 4. The BSW-coupled emission profile (along with the corresponding FS emission profile) that presented maximum emission enhancements in Figure 4b, is shown in Figure 4c. Adopting SC90 in cavity nanointerface aided in accomplishing dequenched as well as enhanced emission enhancements for all the modes sustained by 1DPhC (BSW: 805; IOM_1: 455; IOM_2: 407; IOM_3: 33-fold; IOM_4: 30-fold). The overlap of dispersion diagram obtained numerically (dotted line) and experimentally for AuSC90 cavity layer is shown in Figure 4d (capturing BSW, IOM_1, IOM_2, IOM_3) and in Figure 4e (capturing IOM_4). It is important to note that the IOM_4-coupled emission was not observed with the use of AuNPs and also blank samples. This is because the IOM_4 occurs in the wavelength range from 700 to 760 nm, where the quantum yield of the radiating dipoles (RhB molecules) under consideration is negligible (as the emission profile for RhB is from 540 to 680 nm, with a λ_{max} at 580 nm). Although the emission intensity from RhB is insignificant for >700 nm, we could experimentally observe the coupling of IOM_4 with excellent overlap with numerical data (Figure 4e). Hence, we emphasize that PCCE is the most suitable platform to explore low quantum yield emitters in order to extract reliable and useful information. PCCE profile along with corresponding FS profile for BSW-coupled emission of

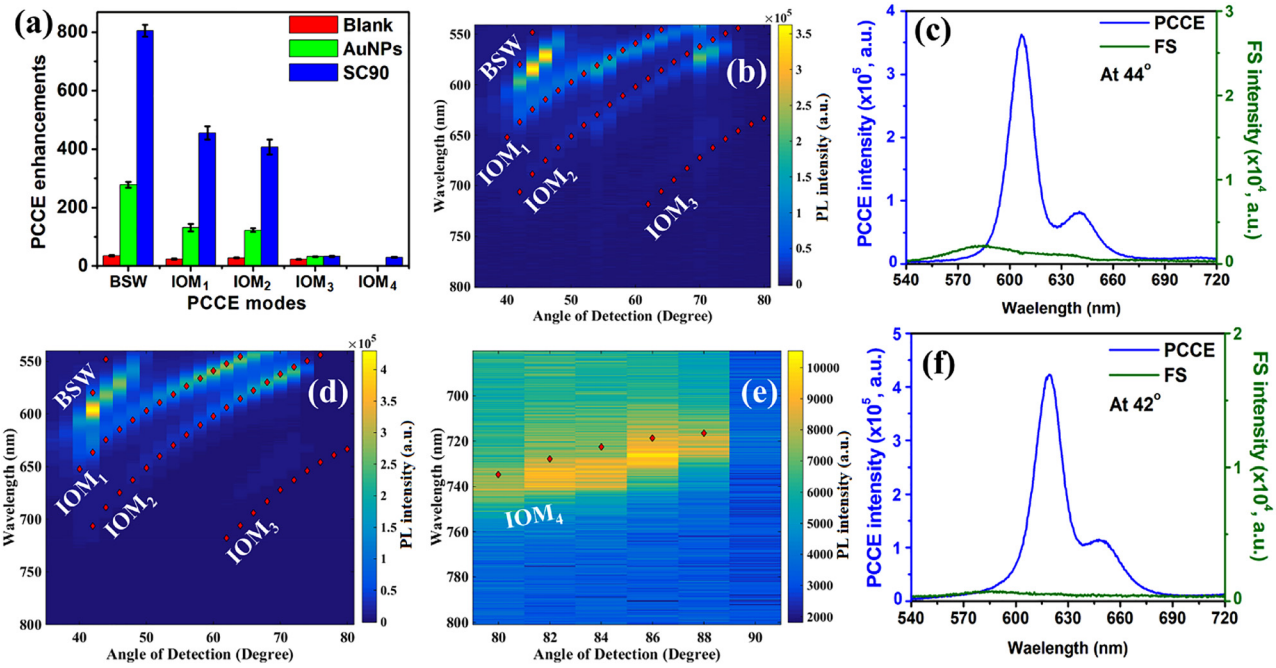

Figure 4: (a) PCCE enhancements for different modes (BSWs, IOM_1, IOM_2, IOM_3 and IOM_4) for blank, AuNPs, SC90 samples. (b) Dispersion diagram presenting overlap of numerical (dotted line for 60 nm PVA) and experimental data for use of 60 nm PVA doped with AuNPs in PCCE platform. (c) PCCE profile along with corresponding FS profile for BSW-coupled emission of (b) that presented maximum emission enhancements with the use of AuNPs. Dispersion diagram presenting overlap of numerical (dotted line for 60 nm PVA) and experimental data for use of 60 nm PVA doped with SC90 in PCCE platform in the angular range (d) 35°–80° and (e) 80°–90°. (f) PCCE profile along with corresponding FS profile for BSW-coupled emission of (d) that presented maximum emission enhancements with the use of SC90. In (b), (d) and (e), the color bar represents fluorescence intensity in arbitrary units and the red dots correspond to the locations of BSW and IOMs from the numerically calculated dispersion diagram.

Figure 4d, that presented maximum emission enhancements with the use of SC90 is shown in Figure 4f. An increase in the PCCE intensity is observed with the use of SC90 (Figure 4d), in comparison with the use of AuNPs (Figure 4c), in line in the emission enhancements presented in Figure 4a.

Earlier report [52], emphasizes on realizing up to 10^5 (in comparison to blank slide) enhancement factor in SERS substrates fabricated on top of 1DPhC using AgNPs. The interplay of plasmonic resonances from NPs and the high EM-field entrapment at the 1DPhC-Ag cavity nanointerface was supported by results from COMSOL® simulations using finite-element method [52]. In line with this, we noted that AgNPs interfaced with 1DPhC, presented augmented emission enhancements that aided in femtomolar sensing of Al^{3+} ions in nanocavity interface [31]. In this context, it is worth mentioning that we have utilized Au sorets for the first time in PCCE platform to realize >800-fold emission enhancements from radiating dipoles in 'photoplasmonic' nanointerface. We have termed it photoplasmonic as the 1DPhC substrate is made up of purely dielectric materials, the AuSC are purely plasmonic nanomaterials. The high enhancements obtained can be attributed to back-and-forth action of several factors at the nanointerface between the AuSC and 1DPhC: (i) Intense BSW and IOM supported by 1DPhC (ii) intra-plasmon coupling between the NPs of a single soret, (iii) inter-plasmon coupling between the adjacently interfaced sorets. As commented earlier, single-molecule detection in PCCE would demand for >1000-fold emission enhancements [32]. We had achieved >1300-fold emission enhancements with the use of integrated hotspots from plasmonic silver nanoprisms (AgNPrs) and dielectric Nd_2O_3 nanorods. This has been used for zeptomolar sensing of biologically relevant cortisol in our recent work [32]. In this context, in the present work we have attempted a seemingly similar, yet markedly different approach to augment the enhancements. Basically, we have two methodologies, namely: (i) generation of intense hotspots using sharp edged plasmonic NPs (AgNPrs) in synergy with anisotropic dielectric NPs (Nd_2O_3 nanorods) of interest [32]; (ii) generation of intense hotspots using stable nanoclusters presenting 3D hotspot density (sorets) in synergy with anisotropic dielectric NPs (Nd_2O_3 nanorods) of interest. While our earlier work [32]; demonstrated the former, here we attempt to understand the utility of latter arrangement. In this context, further experiments were carried out by interfacing 1DPhC with a hybrid mixture of AuSC and Nd_2O_3 NRs and the results are presented in Figure 5.

The conceptual schematic of AuNPs, Nd_2O_3 NRs and AuSC90 under consideration is shown in Figure 5a for easy visualization. The judicious synergy of SC90 and Nd_2O_3 NRs (abbreviated as Nd in figures) resulted in augmented 361-fold emission enhancements (vis-à-vis 161-fold with pristine SC90) in SPCE platform (Figure 5b). SPCE, FS, *p* and *s* emission spectra for sample (SC90 + Nd) presenting maximum enhancements in (b), is shown in Figure 5c. The highly directional emission that could be captured experimentally, with >97% *p*-polarization is presented in Figure 5d. One can note that, the angle of maximum emission has been further increased to 60° (from theoretical 57.3°) with addition of Nd_2O_3 NRs to AuSC (which independently showed directionality at 59°). This is on account of modulation in the effective dielectric constant of the dielectric/PVA layer on top of SPCE substrate, due to doping with NPs. Figure 5f and h presents the numerical dispersion diagram in the angular range from 35° to 80° and 80° to 90° respectively. Here, the color bar represents the reflectance in arbitrary units. Moreover, in order to obtain better comparison, the experimentally obtained fluorescence emission intensity was overlapped with the numerical data (doted plots) for different angular ranges in Figure 5g (35° to 80°) and Figure 5i (80° to 90°). One can note that there is excellent correlation between the experimentally obtained data and numerical simulations. Upon close observation, it can be noted that there is also very good agreement between the intensity of reflectance (Figure 5f and h) and the intensity of fluorescence emission (Figure 5g and i). In other words, for a particular mode (either BSW or IOM), the angle and wavelength where minimum reflectance is observed in simulations, is also the angle where maximum fluorescence is obtained experimentally. A representative plot of experimental data in the angular range from 80° to 90° for SC90 + Nd_2O_3 in PCCE platform for IOM_4 is shown in Figure 5j. This emphasizes that although the quantum yield of RhB emitter in this wavelength range is trivial, on account of integrated hotspots from AuSC-plasmonic nano-assembly, dielectric-Nd_2O_3 NRs and 1DPhC one can distinctly observe the emission profile. The PCCE spectra (corresponding to all dispersion diagrams) obtained with the use of AuNPs, AuSC90 and mixture of AuSC90 + Nd_2O_3, in nanocavity interface, for the complete angular range from 0° to 90° is presented in Supplementary material (Figures S2–S4).

Furthermore, it is important to comment on the nature of the inter plasmon coupling observed in mixture of sorets and Nd_2O_3 NRs. Overall extinction spectra recorded for a particular sample, is a combination of scattering and absorption [52, 53]. Absorption leads to dissipation of incident energy and far-field radiation is an outcome of scattering. Importantly, absorption assists in quenching and scattering aids in improved fluorescence [52, 53]. For nano-

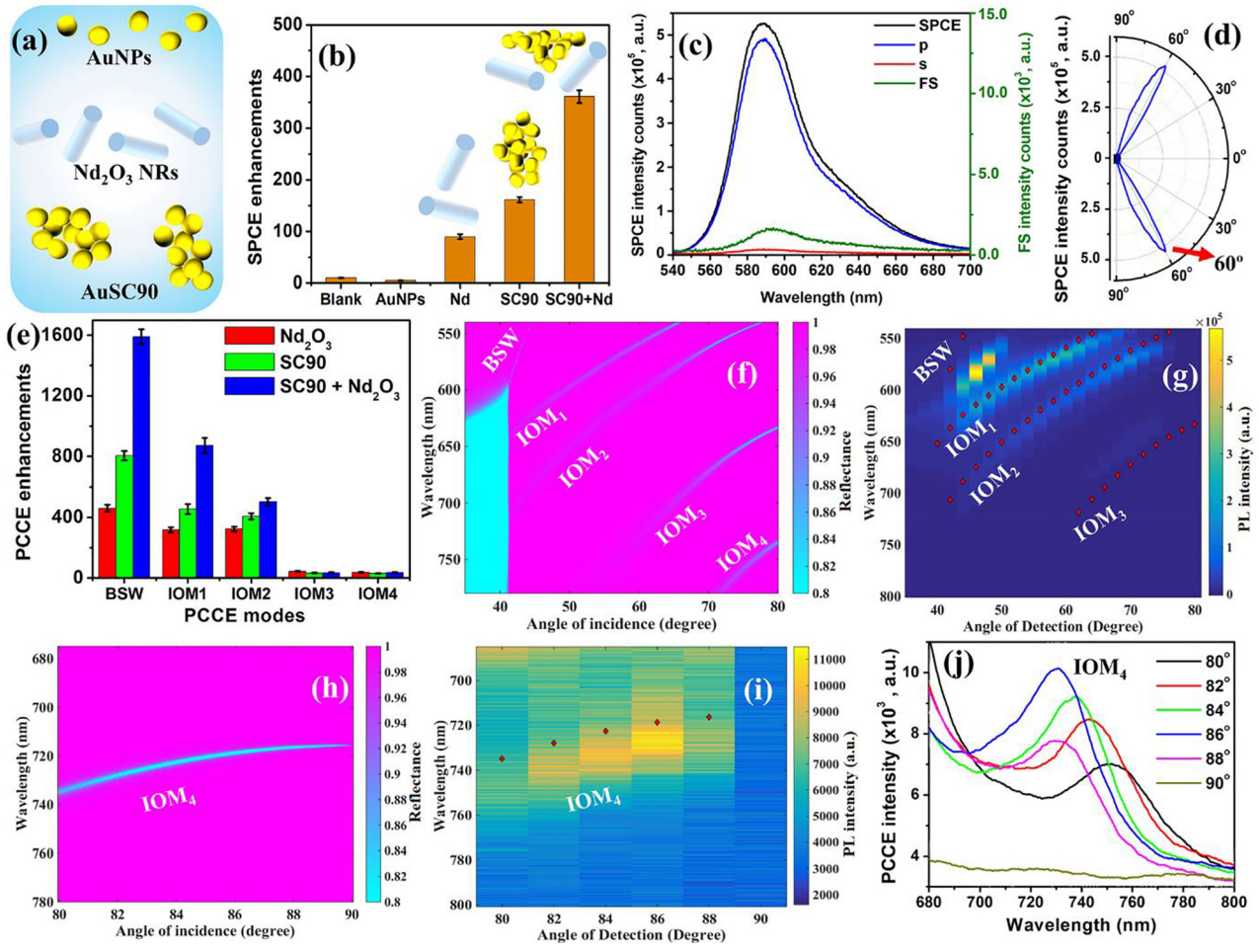

Figure 5: (a) Conceptual schematic of AuNPs, Nd_2O_3 NRs, AuSC90. (b) SPCE enhancements for blank, AuNPs, Nd_2O_3 NRs (Nd), SC90 and mixture of SC90 and Nd in cavity nanointerface. (c) SPCE, Free Space (FS), *p*-polarized (*p*) and *s*-polarized (*s*) emission spectra for sample (SC90 + Nd) presenting maximum enhancements in (b). (d) The corresponding angularity plot (of c) presenting highly directional emission characteristic. (e) PCCE enhancements for different modes (BSWs, IOM_1, IOM_2, IOM_3 and IOM_4) for Nd_2O_3, SC90 and SC90 + Nd_2O_3 samples. (f) Numerical dispersion diagram in the angular range from 35° to 80°. The color bar represents the reflectance in arbitrary units. (g) Dispersion diagram presenting overlap of numerical (dotted line) and experimental data for 60 nm PVA doped SC90 + Nd_2O_3 in PCCE platform. (h) Numerical dispersion diagram in the angular range from 80° to 90°. (i) Dispersion diagram presenting overlap of numerical and experimental data for use of 60 nm PVA doped SC90 + Nd_2O_3 in the angular range from 80° to 90°. (j) The angular sweep from 80° to 90° for SC90 + Nd_2O_3 in PCCE platform. All the remaining PCCE spectra are presented elaborately in SI. In (f) and (h), the color bar represents the reflectance in arbitrary units. In (g) and (i) the color bar represents fluorescence intensity in arbitrary units. The red dots correspond to the locations of BSW and IOMs from the numerically calculated dispersion diagram.

assemblies such as sorets, the UV–Vis absorbance spectra, detailed in our earlier works [33–35] clearly indicates an increase in absorbance at higher wavelength along with spectral broadening as compared to pristine AuNPs. These can be attributed to the enhanced scattering effects from sorets [52, 53]. These nano-assemblies are hence most suitable candidates for metal enhanced fluorescence (MEF) and related studies. Moreover, recently metal-dielectric frameworks are experimentally proven to outperform their purely metal-metal and dielectric-dielectric counterparts [54–57].

In this context, the experimentally observed >1500-fold emission enhancements can be attributed to different factors working in tandem: (i) delocalized void plasmons supported by each soret within the infinitesimal nanogaps in them [21, 40], (ii) localized Mie plasmons supported by entire soret nano-assembly [21, 40], (iii) MEF attributes from sorets on account of enhanced scattering phenomenon [52, 53], (iv) augmented forward scattering of obtained MEF with the help of dielectric HRI Nd_2O_3 NRs [22], (v) metal-dielectric resonances between the plasmonic sorets and dielectric Nd_2O_3 NRs [54–56], (vi) hybrid coupling between BSWs and

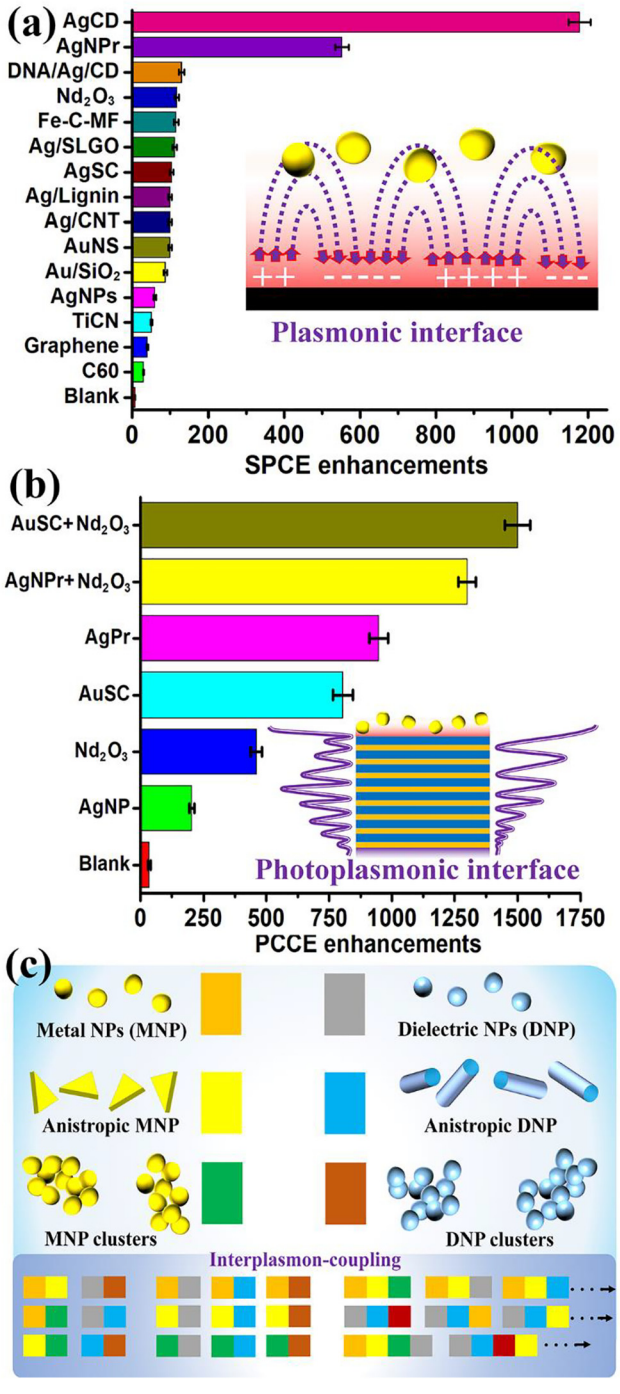

Figure 6: (a) SPCE enhancements obtained with variety of NPs, nanohybrids and composites. The inset shows plasmonic coupling between metal NPs of interest and SPCE substrate. (b) PCCE enhancements obtained with different nanomaterials from our laboratory. >1500-fold experimental PCCE enhancements demonstrated in this work with the use of AuSC (metal) + Nd^2O^3 (dielectric) synergy on 1DPhC nanocavity interface is the maximum that is reported so far. On account of judicious utility of both plasmonic and dielectric frameworks, we have termed this as photoplasmonic interface. (c) A snapshot of the futuristic scope of the photoplasmonic nanointerface indicating different opportunities of combining plasmonic and dielectric materials in SPCE and PCCE platforms. The color shades are used to make the representation much simpler. (Acronyms: AgCD: silver NP decorated-carbon dots; AgNPrs: silver nanoprisms; DNA/Ag/CD: DNA based AgCD composite; Nd_2O_3: neodymium (III) oxide; Ag/SLGO: silver NPs decorated on single layer graphene oxide; Ag/lignin: lignin-based AgNPs; Ag/CNT: carbon nanotubes decorated with AgNPs; AuNS: gold nanostars; Au/SiO_2: gold NPs decorated on silica NPs; TiCN: titanium carbonitride; C60: carbon allotrope or buckminsterfullerene, (C_{60}-I_h)[5, 6] fullerene).

hybridized modes from mixture of sorets and Nd_2O_3 NRs [31, 32, 58]. Moreover, the obtained >1500-fold PCCE enhancements is close to the earlier reported value of 1340-fold fluorescence enhancements in bowtie nanoantennas [50]. In this context, it is worth noting that while the nanoantennas utilized in the earlier work support two-dimensional hotspots, the soret nano-assembly sustains three-dimensional hotspots aiding augmented coupling of emission with the underlying PCCE substrate. Such nano-assemblies in hand with HRI nanorods on a PCCE platform present a synergistic hybrid assembly, on account of which we observed >1500-fold enhancements, presenting coherent and collective plasmonic coupling, that is significantly different from the approach adopted earlier [50]. Additionally, the proposed methodology in this work is a cost-effective technique amenable for developing sensors in resource-limited settings.

In light of these observations, we conclude that the integrated hotspot engineering developed in this work would cater to the immediate requirement of photonic and plasmonic applications. In the previous decade, our laboratory has examined a number of NPs, nanohybrids and nanocomposites to comprehend their plasmonic coupling attributes in SPCE platform. A few of them are presented in Figure 6a, where tunable emission enhancements could be realized with an assortment of nanomaterials (comprising elements from different parts of the periodic table). It is pertinent to note that the maximum emission enhancement that has been realized with SPCE platform is 1000-fold. The PCCE enhancements, obtained with different nanomaterials in cavity nanointerface till date is shown in Figure 6b. It is worth mentioning that this report is the first of its kind presenting >1500-fold emission enhancements.

The main three reasons that assisted in realizing dequenched as well as augmented emission enhancements can be listed as: (i) The modes sustained by the 1DPhC indicates that in these regions the probability of finding the photons are significantly high, especially while the modes are allowed as in the case of BSW and IOMs. As these allowed modes can leak into the substrate in a narrow

cone, it reduces the stringent criteria required for the collection of directional photoluminescence (PL) and therefore can enhance the signal intensity. This is in agreement with the principle of directionality-enhanced PL as a result of which the collection efficiency is also significantly enhanced. (ii) The evanescent field of the BSWs can substantially increase the Purcell factor near the AuSC (nano-assembly), as compared to 1DPhC working in isolation or with that of pristine AuNPs alone. This is on account of the combination of the photonic and plasmonic system in which the combined eigen mode of this hybrid system differs from their singular contributions. (iii) Since the evanescent waves now have large field gradient in the presence of AuSC, it can also couple with its otherwise non-radiative high-order modes to the BSW/SPP. As a consequence of these effects the radiative component of the system is enhanced. In summary, the photonic–plasmonic hybrid architecture of the system is the origin for the observation of dequenched emission.

Moreover, upon close deliberation of Figure 6a and b, one can observe that this report and recent work [32] present just a fraction of possibilities that can be experimentally realized (Figure 6c). Currently, only NPs, metal nanoclusters and anisotropic dielectric NPs are explored in SPCE and PCCE platforms. However, with rapidly growing nanophotonic methodologies for synthesis of NPs and nanoclusters, we anticipate that the proposed photoplasmonic technology would open ample futuristic scope for researchers. Materials display different and useful properties at bulk as well as nanodimensions [59, 60]. A few prudent combinations of anisotropic NPs and their binary, ternary and quaternary nanocomposites would generate nanointerfaces with extremely high EM hotspots for preferred applications. The interplay of sharp nanoedges in anisotropic NPs, nanovoids and nano-crevices in nanoclusters would assist in unravelling the challenging experimental domains, for instance, ‘quenching’ as highlighted in this work. These novel combinations are also subject of fundamental research interest as they eventually impact the probed signal and state of the biomolecule under examination. Some of these studies are underway both theoretically and experimentally, where different desired molecules are conjugated/adsorbed into nanomaterials to fabricate bionanocomplexes with intense hotspots, for immediate utility in biosciences and photonics.

It is informative to briefly discuss the importance of the obtained >1500-fold PCCE enhancements in the perspective of earlier research work carried out on SPCE and PCCE platforms. Since its first report in 2018 [33] soret colloids have been utilized for several sensor applications [21, 23, 33–35]. The SPCE sensor technology has also been utilized for several physico-chemical analysis at plasmonic nanointerfaces [21–24, 29, 50]. The 1000-fold SPCE enhancements realized with AgCD nanohybrids have been used for femtomolar sensing of $LpPLA_2$, a coronary heart disease biomarker. Furthermore, the PCCE platform developed by us has been utilized for sensing aluminium (Al^{3+}) ions and iodide (I^-) ions at femtomolar concentrations for monitoring different disease states [31, 32]. Further, such augmented PCCE enhancements have been utilized for single-molecule detection studies. In this background, here we report the utility of combining the nano-assemblies or soret colloids in PCCE platform to achieve augmented fluorescence enhancements. The unprecedented 1500-fold PCCE enhancements obtained here can be used for detecting ions and molecules at extremely low concentrations. This can be performed by tagging the analytes of interest to fluorophores similar to that reported recently [32], where we detected cortisol at zeptomolar (single-molecule detection) concentration by tagging it to rhodamine B using a simple esterification reaction. Similarly, molecules of interest can also be bio-functionalized on AuNPs of AuSCs and taken forward for sensing applications in different platforms. In addition to this, in this report we noted that PCCE platform engineered with AuSCs presents avenues for detecting fluorescent molecules with very low quantum yield. In summary, one can envisage a wide variety of avenues for monitoring health and disease states using sorets in SPCE and PCCE platforms.

4 Conclusions

Conduction electrons with small ionization energies in metal or plasmonic nanomaterials have emerged as most resourceful factor, supporting interdisciplinary applications. However, the inherent dissipative Ohmic losses hinder their performance. Yet, different plasmonic NPs have stood the test of time, although dielectric NPs and low-dimensional carbon materials have found growing interest and demand in nanophotonic applications. In spite of the fact that plasmonic NPs are extensively explored in SPCE technology, the research pertaining to AuNPs has remained dormant, on account of ‘quenching’ phenomenon. The ‘zone of inactivity’ where the emitters in the vicinity (<5 nm) of AuNPs are broadly believed to be quenched, has been revisited in this work.

In summary, the dual long-standing limitations have been the intrinsic loss in SPCE substrates and quenching with AuNPs. To overcome this predicament, we have utilized the plasmon mixing or interplasmon coupling in the soret nano-geometries of AuNPs along with less-lossy

PCCE platform (analogous to SPCE platform). The individual NPs in sorets interact via optical near fields (generating coupled oscillation modes), presenting multifold hotspots via localized Mie and delocalized Bragg plasmons. Concentrating incident light into highly localized regions (<2 nm) of nearly touching NPs increases the EM field in the gap by several orders of magnitude. We have successfully presented photoplasmonic nanointerface by judicious synergy of plasmonic/metal 3D AuSC nanoassembly and dielectric Nd_2O_3 NRs to achieve >1500-fold emission enhancement in PCCE platform. Nano-assemblies are ideal candidates to efficiently couple propagating light waves into highly localized EM fields, and vice versa. AuSC with 3D morphology presents uniform EM field enhancement across the sample nanointerface, amenable for surface spectroscopies, including SERS, SPCE, PCCE and nonlinear optical techniques. We firmly believe that the research findings presented in this work would furnish immediate requirements of developing integrated hotspots from metal and dielectric NPs in different photonic and plasmonic platforms.

Author contributions: All the authors have accepted responsibility for the entire content of this submitted manuscript and approved submission.

Research funding: S.S.R. and S.B. acknowledge support from Tata Education and Development Trust (TEDT/MUM/HEA/SSSIHL/2017-2018/0069-RM-db), Prasanthi Trust, Inc., USA (22-06-2018), DST-Technology Development Programme (IDP/MED/19/2016), DST-Inspire Research Fellowship (Reg. No. IF180392), Govt. of India. S.B.B.N. acknowledges the support from DST – Advanced Manufacturing Technology Program (DST/TDT/AMT/2017/050). CS and MM acknowledge support from IIT Bombay and DST-Nanomission (SR/NM/TP-56/2012 dated 29-09-2016). "Dr. M. Moronshing and Dr. P. Das contributed equally to this work." Authors thank Sri. Prashant Luthra for proofreading the manuscript. We specially acknowledge Central Research Instruments Facility (CRIF) – SSSIHL for extending the usage of the required instrumentation facility. Guidance from Bhagawan Sri Sathya Sai Baba is gratefully acknowledged.

Conflict of interest statement: The authors declare no conflicts of interest regarding this article.

References

[1] M. Ha, J. H. Kim, M. You, Q. Li, C. Fan, and J. M. Nam, "Multicomponent plasmonic nanoparticles: from heterostructured nanoparticles to colloidal composite nanostructures," *Chem. Rev.*, vol. 119, p. 12208, 2019.

[2] N. Jiang, X. Zhuo, and J. Wang, "Active plasmonics: principles, structures, and applications," *Chem. Rev.*, vol. 118, p. 3054, 2018.

[3] J. R. Lakowicz, K. Ray, M. Chowdhury, et al., "Plasmon-controlled fluorescence: a new paradigm in fluorescence spectroscopy," *Analyst*, vol. 133, p. 1308, 2008.

[4] C. D. Geddes, Ed. *Surface Plasmon Enhanced, Coupled and Controlled Fluorescence*, John Wiley & Sons, 2017.

[5] S. Jahani and Z. Jacob, "All-dielectric metamaterials," *Nat. Nanotechnol.*, vol. 11, p. 23, 2016.

[6] S. Dutta Choudhury, R. Badugu, and J. R. Lakowicz, "Directing fluorescence with plasmonic and photonic structures," *Acc. Chem. Res.*, vol. 48, p. 2171, 2015.

[7] S. Bhaskar, K. N. S. Visweswar, K. M. Ganesh, V. Srinivasan, S. P. Mahesh, and S. S. Ramamurthy, "Metal-free, graphene oxide-based tunable soliton and plasmon engineering for biosensing applications," *ACS Appl. Mater. Interfaces*, vol. 13, p. 17046, 2021.

[8] K. Saha, S. S. Agasti, C. Kim, X. Li, and V. M. Rotello, "Gold nanoparticles in chemical and biological sensing," *Chem. Rev.*, vol. 112, p. 2739, 2012.

[9] M. C. Daniel and D. Astruc, "Gold nanoparticles: assembly, supramolecular chemistry, quantum-size-related properties, and applications toward biology, catalysis, and nanotechnology," *Chem. Rev.*, vol. 104, p. 293, 2004.

[10] C. Kuppe, K. R. Rusimova, L. Ohnoutek, D. Slavov, and V. K. Valev, ""Hot" in plasmonics: temperature-related concepts and applications of metal nanostructures," *Adv. Opt. Mater.*, vol. 8, no. 1, p. 1901166, 2020.

[11] C Clavero, "Plasmon-induced hot-electron generation at nanoparticle/metal-oxide interfaces for photovoltaic and photocatalytic devices," *Nat. Photonics*, vol. 8, p. 95, 2014.

[12] J. F. Li, C. Y. Li, and R. F. Aroca, "Plasmon-enhanced fluorescence spectroscopy," *Chem. Soc. Rev.*, vol. 46, p. 3962, 2017.

[13] I. Gryczynski, J. Malicka, Z. Gryczynski, and J. R. Lakowicz, "Radiative decay engineering 4. Experimental studies of surface plasmon-coupled directional emission," *Anal. Biochem.*, vol. 324, p. 170, 2004.

[14] Y. H. Weng, L. T. Xu, M. Chen, et al., "In situ monitoring of fluorescent polymer brushes by angle-scanning based surface plasmon coupled emission," *ACS Macro Lett.*, vol. 8, p. 223, 2019.

[15] R. Badugu, H. Szmacinski, K. Ray, et al., "Metal-dielectric waveguides for high-efficiency coupled emission," *ACS Photonics*, vol. 2, p. 810, 2015.

[16] Y. Zhao, Y. H. Liu, S. H. Cao, et al., "Excitation-emission synchronization-mediated directional fluorescence: insight into plasmon-coupled emission at vibrational resolution," *J. Phys. Chem. Lett.*, vol. 11, p. 2701, 2020.

[17] S. Rangełowa-Jankowska, D. Jankowski, R. Bogdanowicz, B. Grobelna, and P. Bojarski, "Surface plasmon-coupled emission of rhodamine 110 aggregates in a silica nanolayer," *J. Phys. Chem. Lett.*, vol. 3, p. 3626, 2012.

[18] E. Matveeva, Z. Gryczynski, I. Gryczynski, J. Malicka, and J. R. Lakowicz, "Myoglobin immunoassay utilizing directional surface plasmon-coupled emission," *Anal. Chem.*, vol. 76, p. 6287, 2004.

[19] X. H. Pan, S. H. Cao, M. Chen, et al., "In situ and sensitive monitoring of configuration-switching involved dynamic adsorption by surface

plasmon-coupled directional enhanced Raman scattering," *Phys. Chem. Chem. Phys.*, vol. 22, p. 12624, 2020.
[20] W. H. Koo, S. M. Jeong, S. Nishimura, et al., "Polarization conversion in surface-plasmon-coupled emission from organic light-emitting diodes using spontaneously formed buckles," *Adv. Mater.*, vol. 23, p. 1003, 2011.
[21] S. Bhaskar, M. Moronshing, V. Srinivasan, P. K. Badiya, C. Subramaniam, and S. S. Ramamurthy, "Silver soret nanoparticles for femtomolar sensing of glutathione in a surface plasmon-coupled emission platform," *ACS Appl. Nano Mater.*, vol. 3, p. 4329, 2020.
[22] S. Bhaskar and S. S. Ramamurthy, "Mobile phone-based picomolar detection of tannic acid on Nd_2O_3 nanorod-metal thin-film interfaces," *ACS Appl. Nano Mater.*, vol. 2, p. 4613, 2019.
[23] S. Bhaskar, P. Jha, C. Subramaniam, and S. S. Ramamurthy, "Multifunctional hybrid soret nanoarchitectures for mobile phone-based picomolar Cu^{2+} ion sensing and dye degradation applications," *Phys. E Amsterdam Neth.*, vol. 132, p. 114764, 2021.
[24] V. Srinivasan, A. K. Manne, S. G. Patnaik, and S. S. Ramamurthy, "Cellphone monitoring of multi-qubit emission enhancements from Pd-carbon plasmonic nanocavities in tunable coupling regimes with attomolar sensitivity," *ACS Appl. Mater. Interfaces*, vol. 8, p. 23281, 2016.
[25] S. Dutta Choudhury, R. Badugu, K. Ray, and J. R. Lakowicz, "Steering fluorescence emission with metal-dielectric-metal structures of Au, Ag, and Al," *J. Phys. Chem. C*, vol. 117, p. 15798, 2013.
[26] R. Badugu, E. Descrovi, and J. R. Lakowicz, "Radiative decay engineering 7: Tamm state-coupled emission using a hybrid plasmonic-photonic structure," *Anal. Biochem.*, vol. 445, p. 1, 2014.
[27] G. Schneider, G. Decher, N. Nerambourg, R. Praho, M. H. Werts, and M. Blanchard-Desce, "Distance-dependent fluorescence quenching on gold nanoparticles ensheathed with layer-by-layer assembled polyelectrolytes," *Nano Lett.*, vol. 6, p. 530, 2006.
[28] J. F. Li, Y. J. Zhang, S. Y. Ding, R. Panneerselvam, and Z. Q. Tian, "Core–shell nanoparticle-enhanced Raman spectroscopy," *Chem. Rev.*, vol. 117, p. 5002, 2017.
[29] S. Bhaskar, N. C. S. Kowshik, S. P. Chandran, and S. S. Ramamurthy, "Femtomolar detection of spermidine using au decorated SiO_2 nanohybrid on plasmon-coupled extended cavity nanointerface: a smartphone-based fluorescence dequenching approach," *Langmuir*, vol. 36, p. 2865, 2020.
[30] S. Bhaskar, R. Patra, N. C. S. Kowshik, et al., "Nanostructure effect on quenching and dequenching of quantum emitters on surface plasmon-coupled interface: a comparative analysis using gold nanospheres and nanostars," *Phys. E Amsterdam, Neth.*, p. 114276, 2020, https://doi.org/10.1016/j.physe.2020.114276.
[31] S. Bhaskar, P. Das, V. Srinivasan, BN, S. Bhaktha, and S. S. Ramamurthy, "Bloch surface waves and internal optical modes-driven photonic crystal-coupled emission platform for femtomolar detection of aluminum ions," *J. Phys. Chem. C*, vol. 124, p. 7341, 2020.
[32] S. Bhaskar, A. K. Singh, P. Das, et al., "Superior resonant nanocavities engineering on the photonic crystal-coupled emission platform for the detection of femtomolar iodide and zeptomolar cortisol" *ACS Appl. Mater. Interfaces*, vol. 12, p. 34323, 2020.
[33] M. Moronshing and C. Subramaniam, "Room temperature, multiphasic detection of explosives, and volatile organic compounds using thermodiffusion driven soret colloids," *ACS Sustain. Chem. Eng.*, vol. 6, p. 9470, 2018.
[34] S. Mondal and C. Subramaniam, "Xenobiotic contamination of water by plastics and pesticides revealed through real-time, ultrasensitive, and reliable surface-enhanced Raman scattering," *ACS Sustain. Chem. Eng.*, vol. 8, p. 7639, 2020.
[35] M. Moronshing, S. Bhaskar, S. Mondal, S. S. Ramamurthy, and C. Subramaniam, "Surface-enhanced Raman scattering platform operating over wide pH range with minimal chemical enhancement effects: test case of tyrosine," *J. Raman Spectrosc.*, vol. 50, pp. 826–836, 2019.
[36] H. Yu, Y. Peng, Y. Yang, and Z. Y. Li, "Plasmon-enhanced light–matter interactions and applications," *NPJ Comput. Mater.*, vol. 5, p. 1, 2019.
[37] T. Hutter, F. M. Huang, S. R. Elliott, and S. Mahajan, "Near-field plasmonics of an individual dielectric nanoparticle above a metallic substrate," *J. Phys. Chem. C*, vol. 117, p. 7784, 2013.
[38] G. V. Naik, V. M. Shalaev, and A. Boltasseva, "Alternative plasmonic materials: beyond gold and silver," *Adv. Mater.*, vol. 25, p. 3264, 2013.
[39] P. R. West, S. Ishii, G. V. Naik, N. K. Emani, V. M. Shalaev, and A. Boltasseva, "Searching for better plasmonic materials," *Laser Photonics Rev*, vol. 4, p. 795, 2010.
[40] T. A. Kelf, Y. Sugawara, R. M. Cole, et al., "Localized and delocalized plasmons in metallic nanovoids," *Phys. Rev. B*, vol. 74, p. 245415, 2006.
[41] J. Turkevitch, P. C. Stevenson, and J. Hillier, "A study of the nucleation and growth processes in the synthesis of colloidal gold," *Discuss. Faraday Soc.*, vol. 11, p. 55, 1951.
[42] G. Frens, "Controlled nucleation for the regulation of the particle size in monodisperse gold suspensions," *Nature: Phys. Sci.*, vol. 241, p. 20, 1973.
[43] Y. Kan, F. Ding, C. Zhao, and S. I. Bozhevolnyi, "Directional off-normal photon streaming from hybrid plasmon-emitter coupled metasurfaces," *ACS Photonics*, vol. 7, p. 1111, 2020.
[44] N. Kongsuwan, A. Demetriadou, R. Chikkaraddy, et al., "Suppressed quenching and strong-coupling of purcell-enhanced single-molecule emission in plasmonic nanocavities," *ACS Photonics*, vol. 5, p. 186, 2018.
[45] R. Faggiani, J. Yang, and P. Lalanne, "Quenching, plasmonic, and radiative decays in nanogap emitting devices," *ACS Photonics*, vol. 2, p. 1739, 2015.
[46] J. Yang, R. Faggiani, and P. Lalanne, "Light emission in nanogaps: overcoming quenching," *Nanoscale Horiz.*, vol. 1, p. 11, 2016.
[47] C. Dahmen, B. Schmidt, and G. von Plessen, "Radiation damping in metal nanoparticle pairs," *Nano Lett.*, vol. 7, p. 318, 2007.
[48] A. Bek, R. Jansen, M. Ringler, S. Mayilo, T. A. Klar, and J. Feldmann, "Fluorescence enhancement in hot spots of AFM-designed gold nanoparticle sandwiches," *Nano Lett.*, vol. 8, p. 485, 2008.
[49] M. Blanco-Formoso, N. Pazos-Perez, and R. A. Alvarez-Puebla, "Fabrication and SERS properties of complex and organized nanoparticle plasmonic clusters stable in solution," *Nanoscale*, vol. 12, p. 14948, 2020.
[50] A. Kinkhabwala, Z. Yu, S. Fan, Y. Avlasevich, K. Müllen, and W. E. Moerner, "Large single-molecule fluorescence enhancements produced by a bowtie nanoantenna," *Nat. Photonics*, vol. 3, p. 654, 2009.
[51] A. Rai, S. Bhaskar, and S. S. Ramamurthy, "Plasmon-coupled directional emission from soluplus-mediated AgAu nanoparticles for attomolar sensing using a smartphone," *ACS Appl. Nano Mater.*, vol. 4, p. 5940, 2021.

[52] M. Fränzl, S. Moras, O. D. Gordan, and D. R. Zahn, "Front cover," *J. Phys. Chem. C*, vol. 122, p. 10153, 2018.
[53] J. R. Lakowicz, "Radiative decay engineering 5: metal-enhanced fluorescence and plasmon emission," *Anal. Biochem.*, vol. 337, p. 171, 2005.
[54] P. Dey, T. A. Tabish, S. Mosca, F. Palombo, P. Matousek, and N. Stone, "Plasmonic nanoassemblies: tentacles beat satellites for boosting broadband NIR plasmon coupling providing a novel candidate for SERS and photothermal therapy," *Small*, vol. 16, p. 1906780, 2020.
[55] S. Sun, M. Li, Q. Du, C. E. Png, and P. Bai, "Metal-dielectric hybrid dimer nanoantenna: coupling between surface plasmons and dielectric resonances for fluorescence enhancement," *J. Phys. Chem. C*, vol. 121, p. 12871, 2017.
[56] G. Rui, E. Rusak, I. Staude, et al., "Multipolar coupling in hybrid metal–dielectric metasurfaces," *ACS Photonics*, vol. 3, pp. 349–353, 2016.
[57] S. Sun, L. Wu, P. Bai, and C. E. Png, "Fluorescence enhancement in visible light: dielectric or noble metal?" *Phys. Chem. Chem. Phys.*, vol. 8, p. 19324, 2016.
[58] R. Badugu, K. Nowaczyk, E. Descrovi, and J. R. Lakowicz, "Radiative decay engineering 6: fluorescence on one-dimensional photonic crystals," *Anal. Biochem.*, vol. 442, p. 83, 2013.
[59] P. J. Arathi, S. Bhaskar, R. K. G. Reddy, S. P. Kumar, and V. Ramanathan, "Disulphide linkage: to get cleaved or not? Bulk and nano copper based SERS of cystine," *Spectrochim. Acta Part A*, vol. 196, p. 229, 2018.
[60] P. J. Arathi, S. Bhaskar, R. K. G. Reddy, S. P. Kumar, and V. Ramanathan, "The photocatalytic role of electrodeposited copper on pencil graphite," *Phys. Chem. Chem. Phys.*, vol. 20, p. 3430, 2018.

Supplementary Material: The online version of this article offers supplementary material (https://doi.org/10.1515/nanoph-2021-0124).

Supporting material includes characterization details and methodology adopted for experiments. Raw experimental PCCE spectra obtained with the use of AuNPs, AuSC90 and mixture of AuSC90 + Nd_2O_3, in nanocavity interface, for the complete angular range from 0° to 90° is also presented.